Highly energy-conservative finite difference method for the cylindrical coordinate system

Koji Fukagata∗† and Nobuhide Kasagi∗
∗ *Department of Mechanical Engineering, The University of Tokyo*
7-3-1 Hongo, Bunkyo-ku, Tokyo 113-8656, Japan
† *Institute for Energy Utilization, AIST*
1-2-1 Namiki, Tsukuba-shi, Ibaraki 305-8564, Japan
E-mail: fukagata@thtlab.t.u-tokyo.ac.jp

Version: Published in *J. Comput. Phys.* **181**, 478-498 (2002)
(Received 5 November 2001; revised 3 June 2002)

ABSTRACT

A highly energy-conservative second-order accurate finite difference method for the cylindrical coordinate system is developed. It is rigorously proved that the energy conservation in the discretized space is satisfied when appropriate interpolation schemes are used. This argument holds not only for an unequally-spaced mesh but also for an equally-spaced mesh on the cylindrical coordinates, but not on the Cartesian coordinates. Numerical tests are undertaken for an inviscid flow with different schemes, and it turns out that the proposed scheme offers a superior energy conservation property and greater stability than the intuitive and previously proposed methods, for both equally-spaced and unequally-spaced meshes.

Key Words: Finite difference method; Cylindrical coordinate system; Pipe flow; Incompressible flow; Energy conservation; Advection; Body force; Singularity.

1. INTRODUCTION

With continuous development of high-performance computers, direct numerical simulation (DNS) and large eddy simulation (LES) have become very popular and even inevitable tools for turbulence research [1–4]. In general, the finite difference (FDM) and finite element (FEM) methods are used in these computations, whilst for special configurations with directional homogeneity such as homogeneous turbulence and channel flow very accurate simulation can be performed using the spectral method [5].

One of the most important requirements in FDM-based DNS / LES of incompressible flows is the flux and energy conservation property of the discretized advection terms. Without a sufficient degree of the flux and energy conservation in the discretized space, computations may become unstable and eventually diverge. The idea of energy conservation in the discretized space had already been addressed in the earliest stage of the development of numerical schemes and it had then been applied to establishment of an energy-conservative second-order accurate FDM on an equally-spaced mesh in the Cartesian coordinates [6, 7]. However, for a long while, it had been unclear whether such energy-conservative schemes exist for higher-order finite difference, for unequally-spaced mesh or for coordinate systems other than the Cartesian coordinates.

Recently, Morinishi *et al.* [8] generalized the higher-order finite difference schemes as relevant combinations of second-order finite differences defined on different stencils, and succeeded in developing energy-conservative fourth-order accurate finite difference

schemes on various (regular, staggered, collocate) meshes. On the other hand, Kajishima [9] carefully examined employment of unequally-spaced Cartesian staggered meshes and proposed energy-conservative second-order finite difference schemes for both the gradient and divergence forms of nonlinear terms in Navier-Stokes equation; they are proved to be valid even for unequally-spaced mesh. According to Kajishima's [9] analysis, energy-conservative schemes on an unequally-spaced mesh can be constructed only when relevant interpolation schemes are applied. A similar conclusion concerning the spatial discretization is obtained in the very recent work by Ham et al. [10], who developed an energy conservation scheme also in time discretization.

FDM-based DNS / LES in the cylindrical coordinate system has been reported by several workers. Different schemes have been proposed to remove singularity at the cylindrical axis ($r = 0$). Eggels *et al.* [11] and Akselvoll and Moin [12] used a second-order accurate FDM with a staggered mesh system. They used the primitive variables, i.e., u_r, u_θ, u_z and p, and resolved the singularity by defining the value of u_r at the axis as an average of those at the two grid points sandwiching the axis. Verzicco and Orlandi [13] proposed to use the flux variable in the radial direction, $q_r = (ru_r)$, to avoid calculating u_r at the axis, and demonstrated the validity of their techniques in DNS of turbulent flow in a rotating pipe [14]. Very recently, Constantinescu and Lele [15], based on general series expansion around a singular point, proposed a very accurate treatment at the axis, which is suitable to higher-order FDMs.

In the recent studies of FDM in the cylindrical coordinates [13, 15, 16], focus has been put mainly on the treatment of singularity at the cylindrical axis. Energy conservation in the discretized space such as those made for the Cartesian coordinates, however, has not been discussed in detail. Moreover, advantages and disadvantages of the different schemes proposed, with respect to energy conservation, remain still unclear. Therefore, the objectives of the present study are to examine such energy conservation for the widely used second-order accurate FDM in the cylindrical coordinate system and to propose highly energy-conservative schemes for the advection and centrifugal / Coriolis terms, and also a resolution for the singularity at the axis.

The paper is organized in the following manner. The governing equation in the cylindrical coordinates is introduced in Section 2. In Section 3, mathematical formulation of energy-conservative discretization and interpolation schemes are provided; and a new treatment of the singularity at the axis is proposed in Section 4. The proposed schemes are numerically tested in Section 5. Finally, conclusions are derived in Section 6.

2. GOVERNING EQUATIONS

The governing equations for the motion of an incompressible fluid flow are the continuity and Navier-Stokes equations. In the cylindrical coordinates, these equations read:

- Continuity equation:

$$\frac{1}{r}\frac{\partial(ru_r)}{\partial r} + \frac{1}{r}\frac{\partial u_\theta}{\partial \theta} + \frac{\partial u_z}{\partial z} = 0\,; \tag{1}$$

- Navier-Stokes equation:

$$\begin{cases} \dfrac{\partial u_r}{\partial t} &= h_r + b_r - \dfrac{\partial p}{\partial r} + \dfrac{1}{Re}\left[\dfrac{1}{r}\dfrac{\partial}{\partial r}r\dfrac{\partial u_r}{\partial r} - \dfrac{u_r}{r^2} + \dfrac{1}{r^2}\dfrac{\partial^2 u_r}{\partial \theta^2} + \dfrac{\partial^2 u_r}{\partial z^2} - \dfrac{2}{r^2}\dfrac{\partial u_\theta}{\partial \theta}\right], \\ \dfrac{\partial u_\theta}{\partial t} &= h_\theta + b_\theta - \dfrac{1}{r}\dfrac{\partial p}{\partial \theta} + \dfrac{1}{Re}\left[\dfrac{1}{r}\dfrac{\partial}{\partial r}r\dfrac{\partial u_\theta}{\partial r} - \dfrac{u_\theta}{r^2} + \dfrac{1}{r^2}\dfrac{\partial^2 u_\theta}{\partial \theta^2} + \dfrac{\partial^2 u_\theta}{\partial z^2} + \dfrac{2}{r^2}\dfrac{\partial u_r}{\partial \theta}\right], \\ \dfrac{\partial u_z}{\partial t} &= h_z - \dfrac{dP}{dz} - \dfrac{\partial p}{\partial z} + \dfrac{1}{Re}\left[\dfrac{1}{r}\dfrac{\partial}{\partial r}r\dfrac{\partial u_z}{\partial r} + \dfrac{1}{r^2}\dfrac{\partial^2 u_z}{\partial \theta^2} + \dfrac{\partial^2 u_z}{\partial z^2}\right]. \end{cases} \tag{2}$$

Here, the equations are nondimensionalized by using the pipe diameter R, the characteristic velocity U, and the kinematic viscosity of fluid ν. The Reynolds number is defined by

$$Re = \frac{UR}{\nu}. \tag{3}$$

The characteristic velocity, U, should be defined as either the friction velocity, $u_\tau = \sqrt{\tau_w/\rho}$, or the laminar centerline velocity, U_{lc}, depending on the flow condition, i.e., whether the mean pressure gradient, $-dP/dz$, or the mass flow rate is kept constant over the time of integration.

The first terms, h_r, h_θ and h_z, on the right-hand-side of the Navier-Stokes equation denote the advection terms, i.e.

$$\begin{cases} h_r &= -\dfrac{1}{r}\dfrac{\partial}{\partial r}(ru_ru_r) - \dfrac{1}{r}\dfrac{\partial}{\partial \theta}(u_\theta u_r) - \dfrac{\partial}{\partial z}(u_z u_r), \\ h_\theta &= -\dfrac{1}{r}\dfrac{\partial}{\partial r}(ru_ru_\theta) - \dfrac{1}{r}\dfrac{\partial}{\partial \theta}(u_\theta u_\theta) - \dfrac{\partial}{\partial z}(u_z u_\theta), \\ h_z &= -\dfrac{1}{r}\dfrac{\partial}{\partial r}(ru_ru_z) - \dfrac{1}{r}\dfrac{\partial}{\partial \theta}(u_\theta u_z) - \dfrac{\partial}{\partial z}(u_z u_z). \end{cases} \tag{4}$$

The second terms, b_r and b_θ, in the equations of the r and θ directions are the centrifugal and Coriolis forces arising due to the curvature of the coordinate system, respectively, i.e.,

$$\begin{cases} b_r &= \dfrac{u_\theta^2}{r}, \\ b_\theta &= -\dfrac{u_r u_\theta}{r}. \end{cases} \tag{5}$$

3. RELEVANT SPATIAL DISCRETIZATION AND INTERPOLATION

3.1. Computational mesh

In the present study, we focus only on the most frequently used method — the second-order accurate finite difference scheme with a staggered mesh system. As usual, velocities are defined on the cell surfaces and pressure is defined at the cell centers as shown in Fig. 1. As a practically useful choice, the spacing is assumed to be equal in θ direction and z direction and unequal in r direction. The definition of notations for the positions and mesh spacings in r direction is shown in Fig 2.

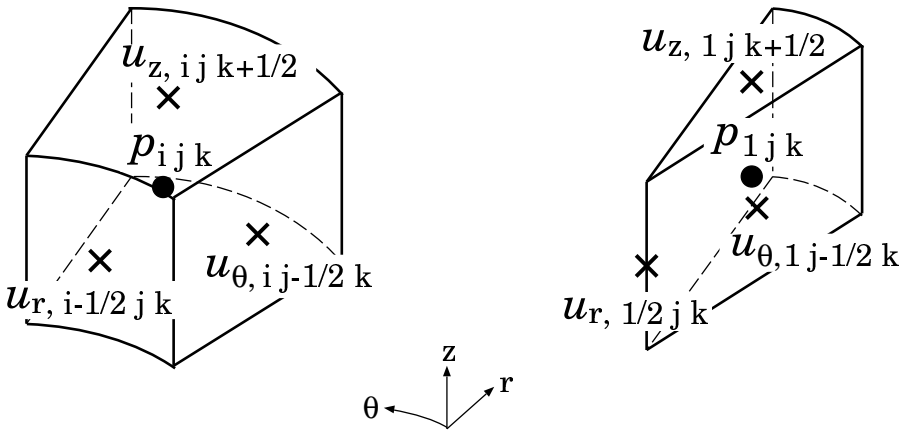

FIG. 1 Definition point of each variable. Ordinary cell (left) and the first cell from the center (right).

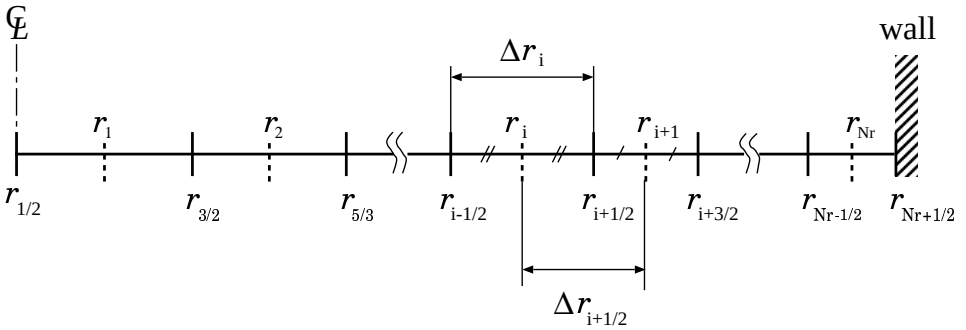

FIG. 2 Definition of the positions, r_i and $r_{i+\frac{1}{2}}$ and the local mesh spacings, Δr_i and $\Delta r_{i+\frac{1}{2}}$.

3.2. Advection term

The advection terms given by Eq. (4) can be discretized so that the flux conservation is satisfied. For instance, the advection term in the r-direction, h_r, can be discretized as:

$$\begin{aligned} h_{r,\,i+\frac{1}{2}\,j\,k} \;=\; & -\frac{1}{r_{i+\frac{1}{2}}}\frac{(ru_r)_{i+1\,j\,k}\,u_{r,\,i+1\,j\,k}-(ru_r)_{i\,j\,k}\,u_{r,\,i\,j\,k}}{\Delta r_{i+\frac{1}{2}}} \\ & -\frac{1}{r_{i+\frac{1}{2}}}\frac{u_{\theta,\,i+\frac{1}{2}\,j+\frac{1}{2}\,k}\,u_{r,\,i+\frac{1}{2}\,j+\frac{1}{2}\,k}-u_{\theta,\,i+\frac{1}{2}\,j-\frac{1}{2}\,k}\,u_{r,\,i+\frac{1}{2}\,j-\frac{1}{2}\,k}}{\Delta\theta} \\ & -\frac{u_{z,\,i+\frac{1}{2}\,j\,k+\frac{1}{2}}\,u_{r,\,i+\frac{1}{2}\,j\,k+\frac{1}{2}}-u_{z,\,i+\frac{1}{2}\,j\,k-\frac{1}{2}}\,u_{r,\,i+\frac{1}{2}\,j\,k-\frac{1}{2}}}{\Delta z}\,, \end{aligned} \tag{6}$$

where $\Delta r_{i+\frac{1}{2}}$ is defined in Fig. 2. The above equation contains undefined velocities such as $u_{r,\,i\,j\,k}$ and $u_{\theta,\,i+\frac{1}{2}\,j+\frac{1}{2}\,k}$. Therefore, we need to evaluate them by interpolation of the defined velocities. A common practice may be to use an arithmetic average or a linear

interpolation. With the arithmetic average, for example, Eq. (6) simply becomes

$$\begin{aligned} h_{r,\,i+\frac{1}{2}\,j\,k} &= -\frac{1}{r_{i+\frac{1}{2}}}\frac{\overline{(ru_r)}^{i}_{i+1\,j\,k}\,\overline{u_r}^{i}_{i+1\,j\,k}-\overline{(ru_r)}^{i}_{i\,j\,k}\,\overline{u_r}^{i}_{i\,j\,k}}{\Delta r_{i+\frac{1}{2}}} \\ &\quad -\frac{1}{r_{i+\frac{1}{2}}}\frac{\overline{u_\theta}^{i}_{i+\frac{1}{2}\,j+\frac{1}{2}\,k}\,\overline{u_r}^{j}_{i+\frac{1}{2}\,j+\frac{1}{2}\,k}-\overline{u_\theta}^{i}_{i+\frac{1}{2}\,j-\frac{1}{2}\,k}\,\overline{u_r}^{j}_{i+\frac{1}{2}\,j-\frac{1}{2}\,k}}{\Delta\theta} \\ &\quad -\frac{\overline{u_z}^{i}_{i+\frac{1}{2}\,j\,k+\frac{1}{2}}\,\overline{u_r}^{k}_{i+\frac{1}{2}\,j\,k+\frac{1}{2}}-\overline{u_z}^{i}_{i+\frac{1}{2}\,j\,k-\frac{1}{2}}\,\overline{u_r}^{k}_{i+\frac{1}{2}\,j\,k-\frac{1}{2}}}{\Delta z}\,, \end{aligned} \tag{7}$$

where the overbar, $\overline{\cdot}^{\ell}$, denotes the arithmetic average and the superscript to the overbar, ℓ, represents the direction of interpolation, e.g.,

$$\begin{aligned} \overline{(ru_r)}^{i}_{i\,j\,k} &= \frac{(ru_r)_{i+\frac{1}{2}\,j\,k}+(ru_r)_{i-\frac{1}{2}\,j\,k}}{2}\,, \\ \overline{u_r}^{j}_{i+\frac{1}{2}\,j+\frac{1}{2}\,k} &= \frac{u_{r,\,i+\frac{1}{2}\,j+1\,k}+u_{r,\,i+\frac{1}{2}\,j\,k}}{2}\,. \end{aligned} \tag{8}$$

However, according to the recent analyses on FDM in the Cartesian coodinates [9, 10, 17], energy conservation is violated in the discretized space when an unequally-spaced mesh is employed and the arithmetic average or the linear interpolation is used on it. This is due to an inconsistency between the differencing and interpolating operators [17]. In order to overcome this problem, Kajishima [9] treated the unequally-spaced rectangular mesh x_m ($m = 1,\ 2,\ 3$) as a mapping from an equally-spaced mesh ξ^m. The divergence form of advection term was approximated by

$$\frac{\partial u_m u_n}{\partial x_n} = \frac{1}{J}\frac{\partial (JU^n u_m)}{\partial \xi^n} = \frac{1}{J}\frac{\delta(\overline{JU^n}^{m}\overline{u_m}^{n})}{\delta\xi^n}\,, \tag{9}$$

where $U^n = u_\ell \partial\xi^n/\partial x_\ell$ is the contravariant velocity and $\delta/\delta\xi^n$ is the second-order central difference on ξ^n mesh. The Jacobian in the mapping is denoted as J. Energy conservation by this approximation was then verified on a two-dimensional Cartesian mesh by the procedure similar to that conducted below. It is also worth noting that such a relevant interpolation rule makes the divergence form and the gradient form of the advection term compatible in the discretized space. This was verified also by that two different numerical simulations of a two-dimensional cavity flow (one of them adopted the divergence form for the nonlinear term; the other, the gradient form) gave the same results. On the other hand, Ham et al. [10] approximated the nonlinear term as

$$\frac{\partial u_m u_n}{\partial x_n} = \frac{\delta \widehat{u_n}^{m}\overline{u_m}^{n}}{\delta x_n} \tag{10}$$

where $\widehat{\cdot}^{\ell}$ is an average weighted by the overlapping volume of the cell where the velocity is defined and of the cell where it is interpolated (referred hereafter as the volume-flux average), and verified the energy conservation property on an unequally-spaced rectangular mesh. It can be easily noticed that these two expressions, Eqs. (9) and (10), are identical when they are expressed in the concrete form in the Cartesian coordinates. Therefore the relevant interpolation schemes for the energy to be conserved can therefore be summarized as:

- volume-flux average — for the *advecting* velocity;
- arithmetic average — for the *advected* velocity.

Here, the terms of *advecting* and *advected* are used for notational convenience. Their meanings are the same as those used for the gradient form of nonlinear terms in the Navier-Stokes equation: in Eq. (6), for example, (ru_r), u_θ and u_z are the *advecting* velocities and u_r is the *advected* velocity.

We apply this interpolation rule to the discretized equation in the cylindrical coordinates. As will be noticed in the verification process below, the key technique (or trick) in the present case is to arrange the right-hand-side in such a form that every term has a common denominator, i.e., $r_{i+\frac{1}{2}}\Delta r_{i+\frac{1}{2}}$. As a result, Eq. (4) reads[1]:

$$\begin{aligned} h_{r,\,i+\frac{1}{2}\;j\,k} \;=\; & -\frac{1}{r_{i+\frac{1}{2}}\Delta r_{i+\frac{1}{2}}}\left[\overline{(ru_r)}^{\,i}_{i+1\;j\,k}\;\overline{u_r}^{\,i}_{i+1\;j\,k}-\overline{(ru_r)}^{\,i}_{i\;j\,k}\;\overline{u_r}^{\,i}_{i\;j\,k}\right] \\ & -\frac{1}{r_{i+\frac{1}{2}}\Delta\theta}\left[\widehat{u_\theta}^{\,i}_{i+\frac{1}{2}\;j+\frac{1}{2}\,k}\;\overline{u_r}^{\,j}_{i+\frac{1}{2}\;j+\frac{1}{2}\,k}-\widehat{u_\theta}^{\,i}_{i+\frac{1}{2}\;j-\frac{1}{2}\,k}\;\overline{u_r}^{\,j}_{i+\frac{1}{2}\;j-\frac{1}{2}\,k}\right] \\ & -\frac{1}{\Delta z}\left[\widehat{u_z}^{\,i}_{i+\frac{1}{2}\;j\,k+\frac{1}{2}}\overline{u_r}^{\,k}_{i+\frac{1}{2}\;j\,k+\frac{1}{2}}-\widehat{u_z}^{\,i}_{i+\frac{1}{2}\;j\,k-\frac{1}{2}}\overline{u_r}^{\,k}_{i+\frac{1}{2}\;j\,k-\frac{1}{2}}\right] \end{aligned} \tag{11}$$

where $\widehat{\cdot}^{\,i}$ denotes the volume-flux average defined by

$$\widehat{u_\theta}^{\,i}_{i+\frac{1}{2}\;j+\frac{1}{2}\,k}=\frac{\Delta r_{i+1}\,u_{\theta,\,i+1\;j+\frac{1}{2}\,k}+\Delta r_i\,u_{\theta,\,i\;j+\frac{1}{2}\,k}}{2\,\Delta r_{i+\frac{1}{2}}} \tag{12}$$

and

$$\widehat{u_z}^{\,i}_{i+\frac{1}{2}\;j\,k+\frac{1}{2}}=\frac{r_{i+1}\Delta r_{i+1}\,u_{z,\,i+1\;j\,k+\frac{1}{2}}+r_i\Delta r_i\,u_{z,\,i\;j\,k+\frac{1}{2}}}{2\,r_{i+\frac{1}{2}}\Delta r_{i+\frac{1}{2}}\chi_{i+\frac{1}{2}}}\,. \tag{13}$$

In the present case, the volume-flux average for (ru_r) is, within second-order accuracy, identical to the arithmetic average for that. The normalization factor, $\chi_{i+\frac{1}{2}}$, in Eq. (13) is necessary so that the summation of the weighting factors becomes unity:

$$\chi_{i+\frac{1}{2}}=\frac{r_{i+1}\Delta r_{i+1}+r_i\Delta r_i}{2\,r_{i+\frac{1}{2}}\Delta r_{i+\frac{1}{2}}}=1+\frac{\Delta r_{i+1}-\Delta r_i}{2r_{i+\frac{1}{2}}}\,, \tag{14}$$

which, of course, is unity for an equally-spaced mesh and close to unity for an unequally-spaced mesh if the variations of Δr in the vicinity of the cylindrical axis is small. Note that the weighting factors due to mesh spacings, Δr_i and Δr_{i+1}, in Eqs. (12) and (13) are opposite to those in the linear interpolation. Moreover, it is emphasized that the present expression, Eq. (11), and that with the arithmetic average, Eq. (7), are not identical even when the mesh spacing is equal, i.e., $\Delta r_i=\Delta r_{i+1}=const.$; the flux weighting factors due to r_i and r_{i+1} still exist in the z-differential term. This situation is quite different from that in the Cartesian coordinate system [9, 10], where the arithmetic average and the relevant interpolation become identical in the case of an equally-spaced mesh.

The terms in other directions, h_θ and h_z, can be discretized similarly. Under the present conditions, i.e., uniform mesh in the θ and z directions, the final expression of h_θ and h_z

[1]There is an obvious typo in the published version (Δ_r should read Δr)

can be obtained using the arithmetic average only. Hereafter, we refer to the form of Eq. (11) as (Div.-C), while the form obtained using the arithmetic average, Eq. (7), is referred to as (Div.-A).

The conservation of a squared value, u_r^2, i.e., a radial component of the kinetic energy, can be verified as follows. Similarly to Eq. (11), the discretized advection term of the squared value can be written as:

$$\begin{aligned} H_{r,\,i+\frac{1}{2}\,j\,k} = & -\frac{1}{r_{i+\frac{1}{2}}\Delta r_{i+\frac{1}{2}}}\left[\overline{(ru_r)}^{i}_{i+1\,j\,k}\,\widetilde{(u_r^2)}^{i}_{i+1\,j\,k} - \overline{(ru_r)}^{i}_{i\,j\,k}\,\widetilde{(u_r^2)}^{i}_{i\,j\,k}\right] \\ & -\frac{1}{r_{i+\frac{1}{2}}\Delta\theta}\left[\widehat{u_\theta}^{i}_{i+\frac{1}{2}\,j+\frac{1}{2}\,k}\,\widetilde{(u_r^2)}^{j}_{i+\frac{1}{2}\,j+\frac{1}{2}\,k} - \widehat{u_\theta}^{i}_{i+\frac{1}{2}\,j-\frac{1}{2}\,k}\,\widetilde{(u_r^2)}^{j}_{i+\frac{1}{2}\,j-\frac{1}{2}\,k}\right] \\ & -\frac{1}{\Delta z}\left[\widehat{u_z}^{i}_{i+\frac{1}{2}\,j\,k+\frac{1}{2}}\widetilde{(u_r^2)}^{k}_{i+\frac{1}{2}\,j\,k+\frac{1}{2}} - \widehat{u_z}^{i}_{i+\frac{1}{2}\,j\,k-\frac{1}{2}}\widetilde{(u_r^2)}^{k}_{i+\frac{1}{2}\,j\,k-\frac{1}{2}}\right] \end{aligned} \tag{15}$$

The squared values at undefined points are evaluated by following Piacsek and Williams [7], e.g.,

$$\begin{aligned} \widetilde{(u_r^2)}_{i,j,k} &= u_{r,\,i+\frac{1}{2}\,j\,k}\,u_{r,\,i-\frac{1}{2}\,j\,k}\,, \\ \widetilde{(u_r^2)}_{i+\frac{1}{2},j+\frac{1}{2},k} &= u_{r,\,i+\frac{1}{2}\,j+1\,k}\,u_{r,\,i+\frac{1}{2}\,j\,k}\,, \\ \widetilde{(u_r^2)}_{i+\frac{1}{2},j,k+\frac{1}{2}} &= u_{r,\,i+\frac{1}{2}\,j\,k+1}\,u_{r,\,i+\frac{1}{2}\,j\,k}\,, \end{aligned} \tag{16}$$

and the normalization factor for the z-differential term, $\chi_{i+\frac{1}{2}}$, was approximated as unity. The transport equation of the squared value can also be obtained by multiplying $2u_{r\,i+\frac{1}{2},j,k}$ to Eq. (11). The former, i.e., Eq. (15), exactly represents the transport of the squared value, whilst the latter, i.e., $2(u_r h_r)_{i+\frac{1}{2}\,j\,k}$, expresses the squared value transport as a result of advection. Therefore, these two expressions must be identical in order for the discretized advection term to become energy-conservative. By subtracting Eq. (15) from $2(u_r h_r)_{i+\frac{1}{2}\,j\,k}$, one obtains

$$2(u_r h_r)_{i+\frac{1}{2}\,j\,k} - H_{r,\,i+\frac{1}{2}\,j\,k} = -\frac{r_{i+1}\Delta r_{i+1}u^2_{r,\,i+\frac{1}{2}\,j\,k}}{2r_{i+\frac{1}{2}}\Delta r_{i+\frac{1}{2}}}(\vec{\mathcal{D}}\cdot\vec{u})_{i+1\,j\,k} - \frac{r_i\Delta r_i u^2_{r,\,i+\frac{1}{2}\,j\,k}}{2r_{i+\frac{1}{2}}\Delta r_{i+\frac{1}{2}}}(\vec{\mathcal{D}}\cdot\vec{u})_{i\,j\,k}\,, \tag{17}$$

where $(\vec{\mathcal{D}}\cdot\vec{u})_{i\,j\,k}$ expresses the divergence of discretized velocity field, i.e,

$$(\vec{\mathcal{D}}\cdot\vec{u})_{i\,j\,k} = \frac{1}{r_i}\frac{(ru_r)_{i+\frac{1}{2}\,j\,k} - (ru_r)_{i-\frac{1}{2}\,j\,k}}{\Delta r_i} + \frac{1}{r_i}\frac{u_{\theta,\,i\,j+\frac{1}{2}\,k} - u_{\theta,\,i\,j-\frac{1}{2}\,k}}{\Delta\theta} + \frac{u_{z,\,i\,j\,k+\frac{1}{2}} - u_{z,\,i\,j\,k-\frac{1}{2}}}{\Delta z}\,. \tag{18}$$

Therefore, the squared value is perfectly conserved if the continuity is satisfied in the discretized space. The equations in the θ and z directions can also be verified likewise.

It should be emphasized again that the scheme based on the arithmetic interpolation, i.e., (Div.-A) expressed by Eq. (7), is not energy-conserving even on the equally-spaced mesh ($\Delta r_i = \Delta r$) in the cylindrical coordinates. A similar analysis as Eqs. (15)-(17) for the

case of (Div.-A) results in

$$2(u_r h_r)_{i+\frac{1}{2}\,j\,k} - H_{r,\,i+\frac{1}{2}\,j\,k} = -\frac{r_{i+1}u^2_{r,\,i+\frac{1}{2}\,j\,k}}{2r_{i+\frac{1}{2}}}(\vec{\mathcal{D}}\cdot\vec{u})_{i+1\,j\,k} - \frac{r_i u^2_{r,\,i+\frac{1}{2}\,j\,k}}{2r_{i+\frac{1}{2}}}(\vec{\mathcal{D}}\cdot\vec{u})_{i\,j\,k} + \frac{\Delta r^2\, u^2_{r,\,i+\frac{1}{2}\,j\,k}}{4r_{i+\frac{1}{2}}}\left.\frac{\delta^2 u_z}{\delta r\delta z}\right|_{i+\frac{1}{2}\,j\,k}, \tag{19}$$

where $\delta/\delta r$ and $\delta/\delta z$ denote the usual second-order central difference. Equation (19) suggests that the energy-conservation property in (Div.-A) on the equally-spaced mesh has a first-order inconsistency near the axis ($r \sim \Delta r$). The similar analysis for other schemes, e.g. (Div.-A) on an unequally-spaced mesh or (Div.-F) appearing in the next section, also reaches the conclusion that $2(u_r h_r)_{i+\frac{1}{2}\,j\,k}$ and $H_{r,\,i+\frac{1}{2}\,j\,k}$ are inconsistent, although the order of inconsistency cannot be expressed in such a simple form as Eq. (19). Therefore, only the combination of discretization and interpolation schemes described above, i.e., (Div.-C). seems to satisfy the conservation of squared values.

3.3. Body force term

The body force terms, b_r and b_θ, satisfy the following relation in the continuous space,

$$u_r b_r + u_\theta b_\theta = 0\,. \tag{20}$$

This relation expresses the exchange of energy between r and θ components. Therefore interpolation for these terms should be designed so as to satisfy this rigorous conservation rule in each 1/4 of a cell as shown in Fig 3. The resulting form, referred to as (Body-C), is

$$\begin{cases} b_{r,\,i+\frac{1}{2}\,j\,k} = \dfrac{1}{r_{i+\frac{1}{2}}}\,\dfrac{\Delta r_{i+1}\overline{(u_\theta^2)}^{\,j}_{i+1\,j\,k} + \Delta r_i \overline{(u_\theta^2)}^{\,j}_{i\,j\,k}}{2\,\Delta r_{i+\frac{1}{2}}}\,, \\ b_{\theta,\,i\,j+\frac{1}{2}\,k} = -\dfrac{1}{r_i}\,\overline{\overline{u_r}^{\,i}}^{\,j}_{i\,j+\frac{1}{2}\,k}\,u_{\theta,\,i,\,j+\frac{1}{2}\,k}\,. \end{cases} \tag{21}$$

Note, again, that the weighting factors are opposite to those in the linear interpolation.

It is unclear what kind of interpolation scheme is used in previous simulation. An intuitive method, however, may be to approximate the undefined velocity simply by using an arithmetic average, which is referred to as (Body-A). In this case, the expression for b_θ is the same as Eq. (21), whilst that for b_r becomes

$$b_{r,\,i+\frac{1}{2}\,j\,k} = \frac{1}{r_{i+\frac{1}{2}}}\left(\overline{\overline{u_\theta}^{\,i}}^{\,j}_{i+\frac{1}{2}\,j\,k}\right)^2. \tag{22}$$

Clearly, the local energy conservation of Eq. (20) is not satisfied by (Body-A), even for the equally-spaced mesh.

4. A NEW TREATMENT AT THE CYLINDRICAL AXIS

As mentioned in the introduction, an important resulting issue in simulation on the cylindrical coordinates is mathematical treatment of the singularity at $r = 0$. Most of the

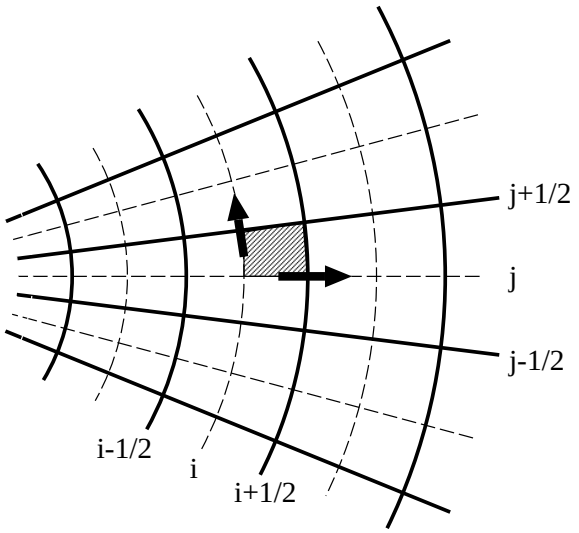

FIG. 3 Subregion of a control volume for u_r and u_θ (shaded). Energy exchange due to body force is conserved in each subregion.

singularities appearing in the Navier-Stokes equation, Eq. (2), are automatically removed after the spatial discretization using second-order FDM with a staggered mesh system. Remaining ones are the radial velocity, $u_{r,\,\frac{1}{2}\,j\,k}$, to be used for:

- interpolation in the advection term, h_r, Eq (11);
- interpolation in the body force term, b_θ, Eq (21);

and that used for discretization of the diffusion terms.

For this problem, two different approaches have been proposed so far as follows:

1. An artificial velocity is defined as:

$$u_{r,\,\frac{1}{2}\,j\,k} = \frac{1}{2}\left(u_{r,\,\frac{3}{2}\,j\,k} - u_{r,\,\frac{3}{2}\,j+\frac{N_\theta}{2}\,k}\right), \tag{23}$$

   where N_θ is the number of mesh in the θ direction (referred to as (Axis-E)) [11];

2. The singularity is removed by multiplying the u_r momentum equation by r (the flux-based formulation) [13].

With the flux-based formulation, h_r and b_θ are discretized as:

$$\begin{aligned}(rh_r)_{i+\frac{1}{2}\,j\,k} \;=\; & -\frac{1}{\Delta r_{i+\frac{1}{2}}}\left[\frac{1}{r_{i+1}}\overline{(ru_r)}^{\,i}_{i+1\,j\,k}\,\overline{(ru_r)}^{\,i}_{i+1\,j\,k} - \frac{1}{r_i}\overline{(ru_r)}^{\,i}_{i\,j\,k}\,\overline{(ru_r)}^{\,i}_{i\,j\,k}\right] \\ & -\frac{1}{r_{i+\frac{1}{2}}}\frac{\overline{u_\theta}^{\,i}_{i+\frac{1}{2}\,j+\frac{1}{2}\,k}\,\overline{(ru_r)}^{\,j}_{i+\frac{1}{2}\,j+\frac{1}{2}\,k} - \overline{u_\theta}^{\,i}_{i+\frac{1}{2}\,j-\frac{1}{2}\,k}\,\overline{(ru_r)}^{\,j}_{i+\frac{1}{2}\,j-\frac{1}{2}\,k}}{\Delta\theta} \\ & -\frac{\overline{u_z}^{\,i}_{i+\frac{1}{2}\,j\,k+\frac{1}{2}}\,\overline{(ru_r)}^{\,k}_{i+\frac{1}{2}\,j\,k+\frac{1}{2}} - \overline{u_z}^{\,i}_{i+\frac{1}{2}\,j\,k-\frac{1}{2}}\,\overline{(ru_r)}^{\,k}_{i+\frac{1}{2}\,j\,k-\frac{1}{2}}}{\Delta z},\end{aligned} \tag{24}$$

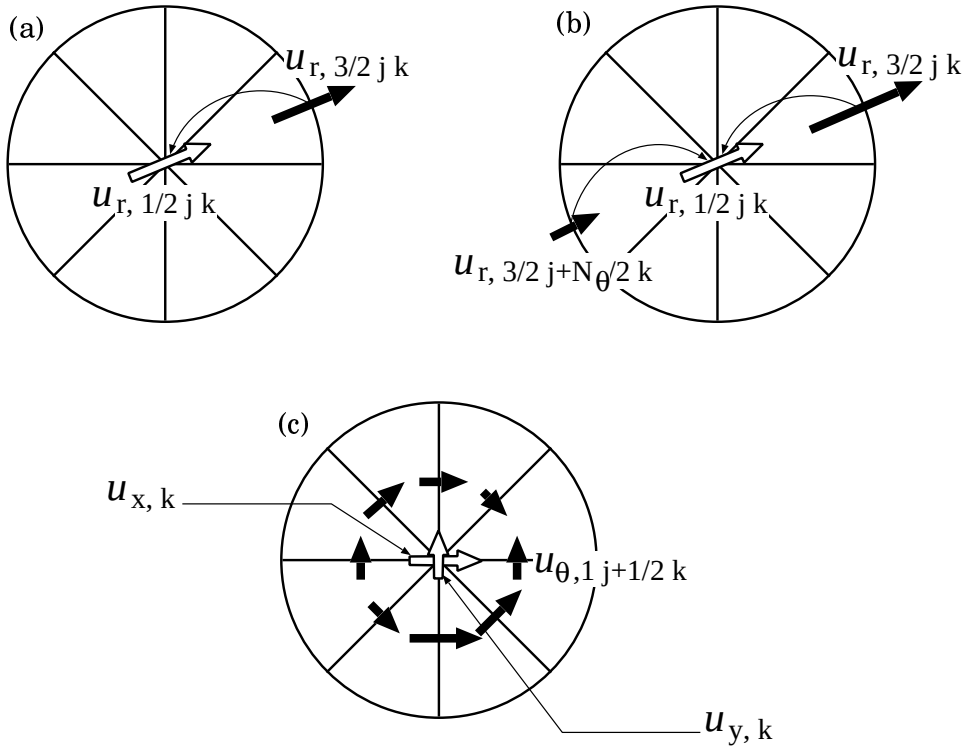

FIG. 4 Different treatments at cylindrical axis. Vectors in black are those defined and actually solved; vectors in white are artificial ones at $r = 0$. (a) method equivalent to flux-based formulation (Axis-F); (b) treatment by Eggels et al. (1994) (Axis-E); (c) first step of the present method (Axis-C).

and

$$b_{\theta,\, i\, j+\frac{1}{2}\, k} = -\frac{1}{r_i^2}\, \overline{\overline{(ru_r)}^{i}}^{j}_{\,i\, j+\frac{1}{2}\, k}\, u_{\theta,\, i,\, j+\frac{1}{2}\, k}\,. \tag{25}$$

Since $(ru_r)_{\frac{1}{2}\, j\, k} = 0$, it does not require any approximation at the point of $r = 0$. However, based on this formulation, an energy-conservative scheme such as one in the previous section cannot be constructed. A modified method, in which the energy-conservative scheme is used, but with the flux-based formulation only at the first points from the axis, can also be considered. In that case, it can be found from Eq. (11) that it is equivalent to use the following artificial velocity (referred to as (Axis-F)):

$$u_{r,\, \frac{1}{2}\, j\, k} = u_{r,\, \frac{3}{2}\, j\, k}\,. \tag{26}$$

A schematic of the different treatments is shown in Fig. 4.

In the present study, a new method is proposed such that the mathematical constraint at $r = 0$:

$$\begin{cases} u_r &= u_x \cos\theta + u_y \sin\theta\,, \\ u_\theta &= -u_x \sin\theta + u_y \cos\theta\,, \end{cases} \tag{27}$$

should be satisfied. Here, u_x and u_y are velocity components expressed in the Cartesian coordinates. As shown in Fig. 4c, the procedure to compute $u_{r,\, \frac{1}{2}\, j\, k}$ is given as follows:

1. calculate u_x and u_y at $r=0$ from $u_{\theta,\,1\,j+\frac{1}{2}\,k}$[2]:

$$\left\{\begin{array}{rcl} u_{x,\,k} &=& -\dfrac{2}{N_\theta}\displaystyle\sum_{j=0}^{N_\theta-1} u_{\theta,\,1\,j+\frac{1}{2}\,k}\sin\theta_{j+\frac{1}{2}}\,, \\ u_{y,\,k} &=& \dfrac{2}{N_\theta}\displaystyle\sum_{j=0}^{N_\theta-1} u_{\theta,\,1\,j+\frac{1}{2}\,k}\cos\theta_{j+\frac{1}{2}}\,. \end{array}\right. \tag{28}$$

2. calculate $u_{r,\,\frac{1}{2}\,j\,k}$ by using Eq. (27):

$$u_{r,\,\frac{1}{2}\,j\,k} = u_{x,\,k}\cos\theta_j + u_{y,\,k}\sin\theta_j\,. \tag{29}$$

The accuracy order of the present procedure can easily be assessed. The series expansion of $u_{\theta,\,1\,j+\frac{1}{2}\,k}$, around the singular point, $r=0$, can be written [15, 18] as:

$$\begin{aligned} u_{\theta,\,1\,j+\frac{1}{2}\,k} &= A_{01}^{(\theta)}\left(\frac{\Delta r_1}{2}\right)+\left[A_{10}^{(\theta)}+A_{11}^{(\theta)}\left(\frac{\Delta r_1}{2}\right)^2\right]\cos\theta_{j+\frac{1}{2}}+A_{20}^{(\theta)}\left(\frac{\Delta r_1}{2}\right)\cos 2\theta_{j+\frac{1}{2}} \\ &\quad +B_{01}^{(\theta)}\left(\frac{\Delta r_1}{2}\right)+\left[B_{10}^{(\theta)}+B_{11}^{(\theta)}\left(\frac{\Delta r_1}{2}\right)^2\right]\sin\theta_{j+\frac{1}{2}}+B_{20}^{(\theta)}\left(\frac{\Delta r_1}{2}\right)\sin 2\theta_{j+\frac{1}{2}} \\ &\quad +O(\Delta r_1^3)\,, \end{aligned} \tag{30}$$

where $A_{mn}^{(\theta)}$ and $B_{mn}^{(\theta)}$ are coefficients for the corresponding modes. It is easily found that $A_{10}^{(\theta)}$ and $B_{10}^{(\theta)}$ are equivalent, respectively, to

$$\left\{\begin{array}{rcl} A_{10}^{(\theta)} &=& u_{y,\,k}\,, \\ B_{10}^{(\theta)} &=& -u_{x,\,k}\,. \end{array}\right. \tag{31}$$

Summation of Eq. (30) multiplied by $\cos\theta$ yields

$$\sum_{j=0}^{N_\theta-1} u_{\theta,\,1\,j+\frac{1}{2}\,k}\cos\theta_{j+\frac{1}{2}} = \frac{N_\theta}{2}\left[u_{y,\,k}+A_{11}^{(\theta)}\left(\frac{\Delta r_1}{2}\right)^2\right]\,. \tag{32}$$

Similarly,

$$\sum_{j=0}^{N_\theta-1} u_{\theta,\,1\,j+\frac{1}{2}\,k}\sin\theta_{j+\frac{1}{2}} = \frac{N_\theta}{2}\left[-u_{x,\,k}+B_{11}^{(\theta)}\left(\frac{\Delta r_1}{2}\right)^2\right]\,. \tag{33}$$

Therefore, the present interpolation procedure, Eq. (28), has second-order accuracy with respect to Δr_1.

Energy conservation around the cylindrical axis should also be investigated. By carrying out derivation similar to that in the previous section, we find that an extra condition,

$$u_{r,\,\frac{3}{2}\,j\,k}+\frac{u_{\theta,\,1\,j+\frac{1}{2}\,k}-u_{\theta,\,1\,j-\frac{1}{2}\,k}}{\Delta\theta}=0\,, \tag{34}$$

[2]There are typos in the published version (subscript to θ_j).

should be satisfied in order for the squared value to be conserved. From the series expansion similar to Eq. (30), one obtains

$$u_{r,\,\frac{3}{2}\,j\,k}+\frac{u_{\theta,\,1\,j+\frac{1}{2}\,k}-u_{\theta,\,1\,j-\frac{1}{2}\,k}}{\Delta\theta} = \left[A_{01}^{(r)}+B_{01}^{(r)}+(A_{20}^{(r)}-A_{20}^{(\theta)})\cos 2\theta_j+(B_{20}^{(r)}-B_{20}^{(\theta)})\sin 2\theta_j\right]\Delta r_1+O(\Delta r_1^2,\,\Delta\theta^2)\,, \tag{35}$$

which reveals that the present method has only first-order accuracy concerning the energy conservation around the cylindrical axis. However, we do not attempt to directly impose the condition of Eq. (34), because such or an equivalent condition under the continuity,

$$u_{z,\,1\,j\,k+\frac{1}{2}}-u_{z,\,1\,j\,k-\frac{1}{2}}=0\,, \tag{36}$$

prohibits any variation of u_z along the longitudinal direction and is quite unphysical. The effects of this first-order error around the axis are shown to be minor in the next section because the size of volume influenced is considered small if compared to the rest of the domain.

5. NUMERICAL TEST

In order to demonstrate an energy conservation property of the proposed schemes, numerical tests are conducted assuming an inviscid flow in a straight circular pipe, i.e., $Re\to\infty$, with no driving force, i.e., $-dP/dz=0$. The reduced set of governing equations read:

- continuity equation:
$$\frac{1}{r}\frac{\partial(ru_r)}{\partial r}+\frac{1}{r}\frac{\partial u_\theta}{\partial\theta}+\frac{\partial u_z}{\partial z}=0\,; \tag{37}$$
- momentum equation:
$$\begin{cases} \dfrac{\partial u_r}{\partial t} &= h_r+b_r-\dfrac{\partial p}{\partial r}\,, \\ \dfrac{\partial u_\theta}{\partial t} &= h_\theta+b_\theta-\dfrac{1}{r}\dfrac{\partial p}{\partial\theta}\,, \\ \dfrac{\partial u_z}{\partial t} &= h_z-\dfrac{\partial p}{\partial z}\,. \end{cases} \tag{38}$$

Tested different combinations of schemes for the advection term, body force term and treatment at the axis are summarized in the following:

- advection term
  - (Div.-C) present scheme, Eq. (11),
  - (Div.-A) arithmetic average, Eq. (7),
  - (Div.-F) flux-based formulation, Eq. (24),
- body force term
  - (Body-C) present scheme, Eq. (21),

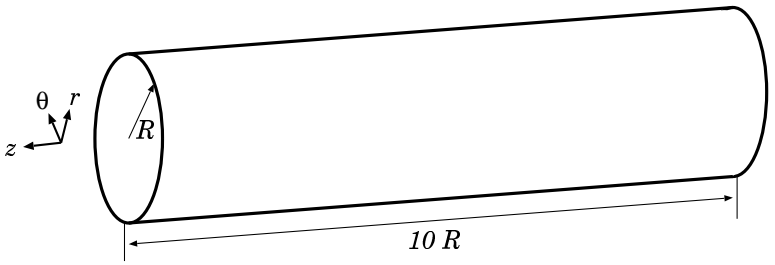

FIG. 5 Computational domain.

  - (Body-A) arithmetic average, Eq. (22),
  - (Body-F) flux-based formulation, Eq. (25),

- treatment at the cylindrical axis
  - (Axis-C) present procedure, Eqs. (28)-(29),
  - (Axis-E) treatment by Eggels *et al.* (1994), Eq. (23),
  - (Axis-F) method equivalent to flux-based formulation, Eq. (26).

The computational domain has a radius of $R = 1$ and a length of $10\,R$ as shown in Fig. 5 and periodic boundary condition is applied at both ends. Equally-spaced and unequally-spaced computational meshes are tested. The number and the sizes of the computational mesh used in the main test are tabulated in Table 1. The initial velocity field, with which the time advancing integration is started, is generated in the following way:

1. interpolate velocities from an instantaneous velocity field of fully developed turbulent pipe flow at $Re_\tau = 180$ simulated on a $96 \times 128 \times 256$ mesh (see Appendix A) onto the mesh (8 times coarser in each direction) used for the tests;

2. solve the Poisson equation in order for the reduced velocity field to satisfy the continuity equation;

3. normalize the velocities to have zero mean velocity, i.e. $< u_r >=< u_\theta >=< u_z >= 0$, and unit kinetic energy, i.e. $< k >=< \frac{1}{2}(u_i u_i) >= 1$.

The procedure employed here is similar to that used by Morinishi *et al.* [8], who used a random stream function in a two-dimensional problem. Instead of using random vector potential as a seed, DNS data is used to obtain an organized three-dimensional velocity field.

TABLE 1
Computational mesh used in the numerical test. Sizes are nondimensionalized by R. Normalization factor, χ, is defined in Eq. (14).

Notation	N_r	N_θ	N_z	Δr	$\Delta\theta$	Δz	χ
equally-spaced	12	16	32	0.083	0.39	0.31	1.00
unequally-spaced	12	16	32	0.021 - 0.13	0.39	0.31	0.83 - 1.00

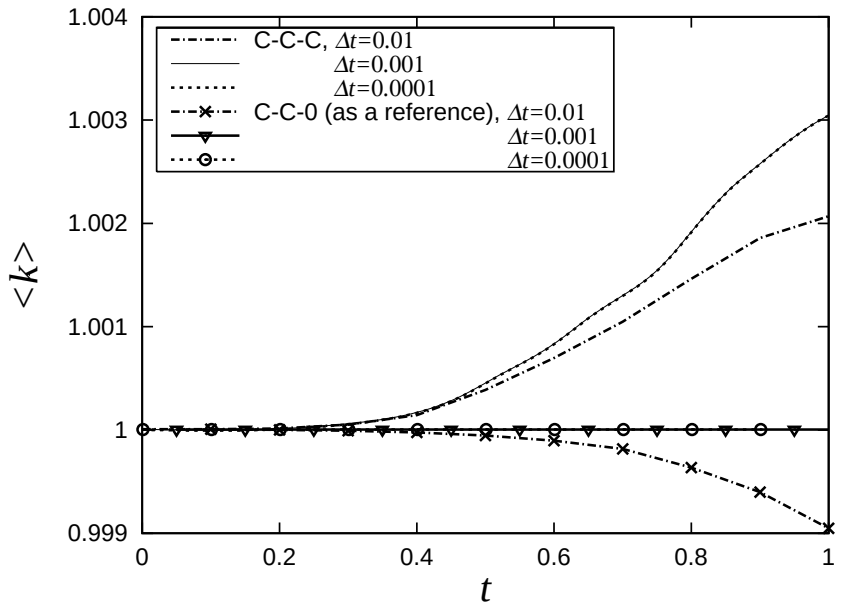

FIG. 6 Time trace of the total kinetic energy $< k >$ computed with different time steps. Energy conservative scheme with (Div.-C)-(Body-C)-(Axis-C) (key "C-C-C") and that with $u_r(0,\ \theta,\ z) = 0$ boundary condition ("C-C-0") were used on equally-spaced mesh.

Time integration of the discretized equation is achieved by using the low storage third-order Runge-Kutta scheme [19]. The same coefficients as those used by Rai and Moin [20] are used. For the pressure coupling, a delta-form fractional step method, which can be found in [13, 21], is used. The Poisson equation is solved using trigonometric expansions.

Even if the spatial discretization ideally satisfies the energy conservation, the energy may change due to the imperfectness of a time integration scheme. Therefore, a preliminary test is made with different computational time steps of Δt=0.01, 0.001 and 0.0001. The combination of the proposed schemes, i.e., (Div.-C)-(Body-C)-(Axis-C), was used. As was discussed in the previous section, (Axis-C) has an imperfect (lower-order accuracy) energy conservation property. Therefore, a case with a boundary condition of $u_r(0,\ \theta,\ z) = 0$, denoted as (Axis-0), was also tested in order to examine the case where the problem of the axis treatment is absent. The result is given in Fig. 6, where Δt=0.001 and 0.0001 give the indistinguishable results of the kinetic energy, $< k >$. Due to the dissipative nature of the Runge-Kutta time integration scheme, $< k >$ should decrease with time and the rate of decrease should be higher for larger Δt. The result for the reference case, i.e., (Div.-C)-(Body-C)-(Axis-0), properly shows such a trend. For (Div.-C)-(Body-C)-(Axis-C), however, the kinetic energy increased due to the imperfect conservation in the treatment of the axis. The smaller increase of $< k >$ in the case of $\Delta t = 0.01$ is consistent with the dissipative nature of the time integration scheme. Throughout the following test, the time step is fixed at $\Delta t = 0.001$ except for the test on the different amplitude of initial perturbation and grid resolution where the Courant number is set approximately the same as this condition.

The test is initiated from the case of the equally-spaced mesh. Figure 7 shows the time trace of $< k >$ in the case of the equally-spaced mesh. The kinetic energy should be unchanged as time advances, because the governing equation does not have any source and dissipative terms. According to Fig. 7a, the energy is kept almost constant regardless of

(a)

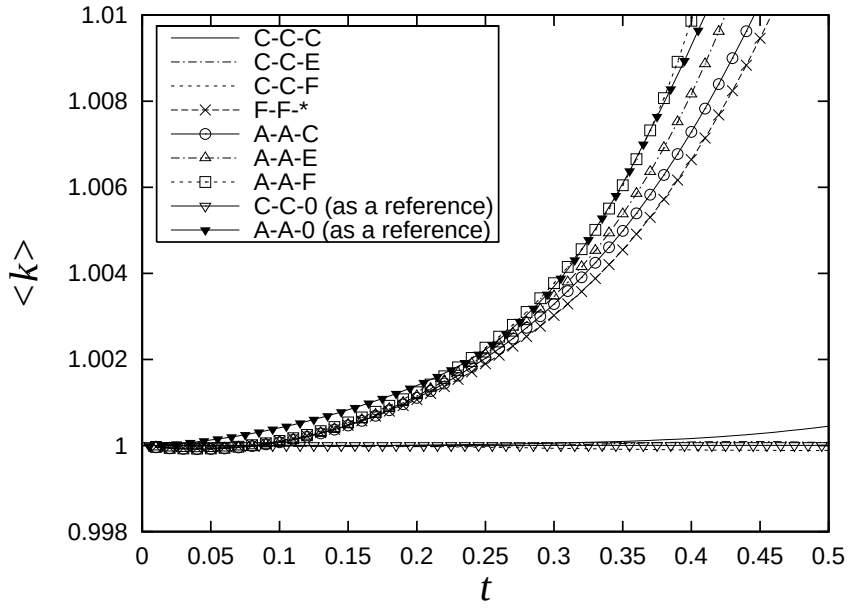

(b)

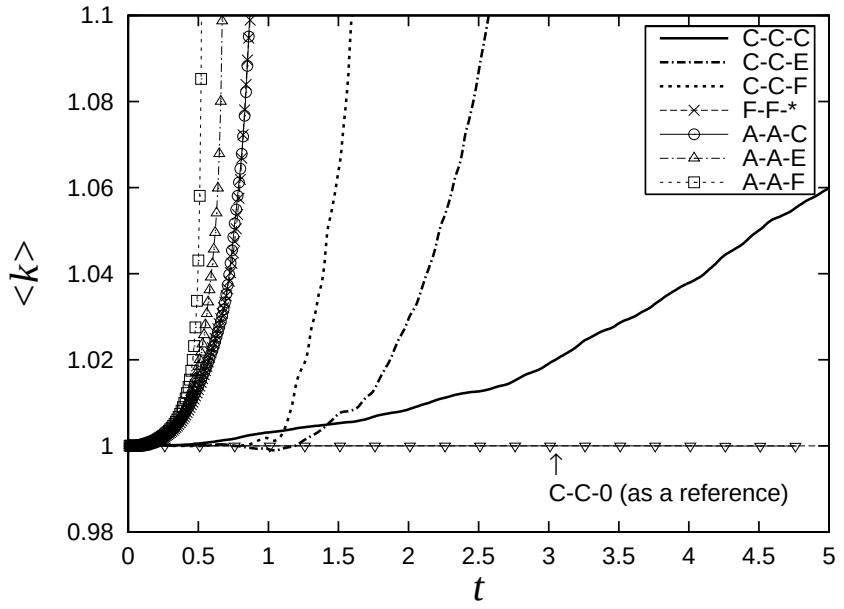

FIG. 7 Time trace of the total kinetic energy $< k >$ computed using different methods. (a) initial period until $t = 0.5$; (b) for longer period until $t = 5$. Equally-spaced mesh and Δt=0.001 are employed. Key "C-C-E" denotes a combination of (Div.-C)-(Body-C)-(Axis-E), and similar abbreviations apply to other combinations.

TABLE 2
The time when the error in total kinetic energy grows to 1 %, denoted as $T_{1\%}$, that to 50 %, $T_{50\%}$, and the time when the computation diverges, T_{div}. Equally-spaced mesh and Δt=0.001 are employed.

Advection term	Body force term	Treatment at axis	$T_{1\%}$	$T_{50\%}$	T_{div}
(Div.-C)	(Body-C)	(Axis-C)	2.16	16.08	65.62
(Div.-C)	(Body-A)	(Axis-C)	0.81	4.97	15.22
(Div.-C)	(Body-C)	(Axis-E)	1.67	3.50	5.59
(Div.-C)	(Body-C)	(Axis-F)	1.18	1.93	2.34
(Div.-F)	(Body-F)	$*$	0.46	1.25	1.36
(Div.-A)	(Body-A)	(Axis-C)	0.45	1.02	1.12
(Div.-A)	(Body-C)	(Axis-C)	0.44	0.82	0.86
(Div.-A)	(Body-A)	(Axis-E)	0.43	0.71	0.75
(Div.-A)	(Body-A)	(Axis-F)	0.41	0.55	0.56

differences in the treatment at the cylindrical axis when the present schemes, (Div-.C) and (Body-C), are used. On the other hand, the increase of $< k >$ is remarkable in the cases of arithmetic average, (Div.-A) and (Body-A), and of the flux-based formulation, (Div.-F) and (Body-F). Over longer time of integration, the increase of $< k >$ is discernible in all cases of combination, as shown in Fig. 7b. The present combination, (Div.-C)-(Body-C)-(Axis-C), exhibits the least error in the energy conservation property and the highest stability. The gradual increase of $< k >$ even for the best scheme, again, can be attributed to the imperfect energy conservation around the cylindrical axis as can be noticed from the result of (Div.-C)-(Body-C)-(Axis-0) also drawn in Fig. 7b as a reference.

As convenient measures of the energy conservation and of the computational stability, we introduce the time when the error in total kinetic energy grows to 1 %, denoted as $T_{1\%}$, that to 50 %, $T_{50\%}$, and that when the computation to diverges, T_{div}. They are tabulated in Table 2. Again, the combination of the present schemes, (Div.-C)-(Body-C)-(Axis-C), is far superior to other combinations. The energy conservation property is more sensitive to the scheme used for the advection and body force terms than to the treatment at the axis. Moreover, it is noticed from the comparison between (Div.-C)-(Body-A)-(Axis-C) and (Div.-A)-(Body-C)-(Axis-C) that the energy conservation of the advection term is more important than that of the body force term.

Dependency of the energy conservation property in an initial period, $t = 0.25$ (corresponding to the center of Fig. 7a), on the amplitude of initial perturbation, $< k >_{init}$, and the grid resolution, Δr, is depicted in Fig. 8. The error, ε, is defined as

$$\varepsilon = \frac{< k >_{t=0.25} - < k >_{init}}{< k >_{init}} . \tag{39}$$

It is reconfirmed that the error of the proposed scheme, i.e., (Div.-C)-(Body-C)-(Axis-C), is much smaller than that of the intuitive scheme, i.e., (Div.-A)-(Body-A)-(Axis-C), for any $< k >_{init}$ and Δr. The error decreases as $< k >_{init}$ or Δr becomes smaller. The energy conservation property of the present scheme is found to be between first and second order in terms of Δr which reflects the order of inconsistency in (Axis-C). It should be noted that the error in the reference case, (Div.-C)-(Body-C)-(Axis-0), is much smaller and the most of that error is likely caused by the time integration ($\varepsilon \simeq -3 \times 10^{-8}$ for $< k >_{init} = 1$ and

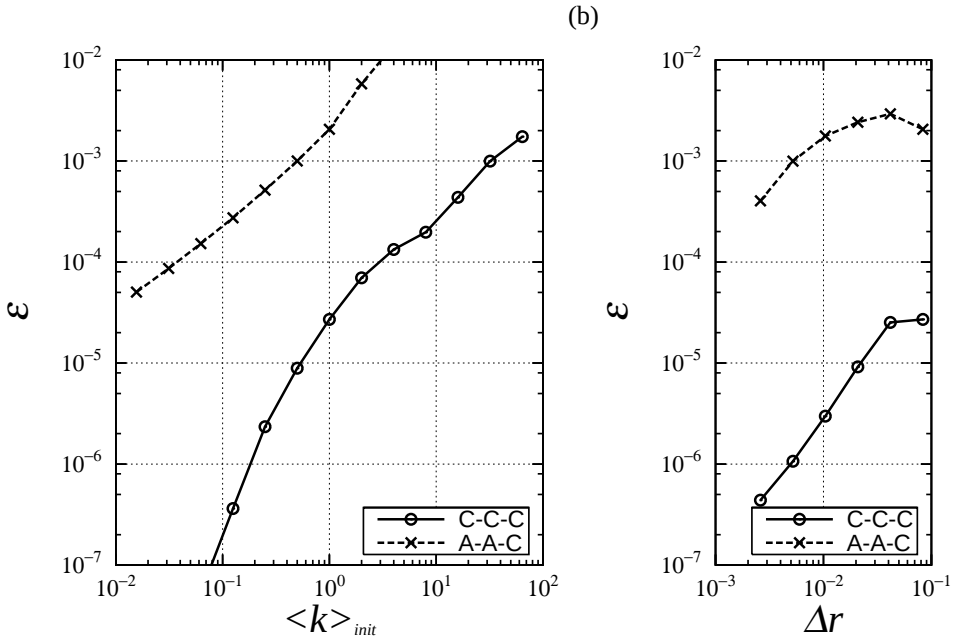

FIG. 8 Dependency of the error in kinetic energy in an initial period ($t = 0.25$). (a) On the amplitude of initial perturbation; (b) On the grid size.

$\Delta r \simeq 0.083$).

Subsequently, a test on the unequally-spaced mesh is performed with the default conditions, i.e., $< k >_{init} = 1$ and the mesh shown in Table 1. As summarized in Table 3, the results are similar to those for the equally-spaced mesh. Energy conservation property of the present scheme for advection term is quite well despite the approximation of $\chi = 1$ made in the verification process, Eqs. (15)-(17), and the superiority of the combination of the present schemes is even more clearer. Given the comparison between Tables 2 and 3, one may wonder why the error computed using the present schemes grows slower on the unequally-spaced mesh. Note that these two results cannot directly be compared because the smoothness of the initial fields is different. Comparison between tests with different mesh sizes is not straightforward in the case of unequally-spaced mesh and thus omitted. However, it is apparent from Eqs. (7) and (11) that difference between the intuitive scheme

TABLE 3

The time when the error in total kinetic energy grows to 1 %, $T_{1\%}$, that to 50 %, $T_{50\%}$, and the time when the computation diverges, T_{div}. Unequally-spaced mesh and Δt=0.001 are employed.

Advection term	Body force term	Treatment at axis	$T_{1\%}$	$T_{50\%}$	T_{div}
(Div.-C)	(Body-C)	(Axis-C)	2.71	34.16	167.13
(Div.-F)	(Body-F)	$*$	0.50	1.47	1.52
(Div.-A)	(Body-A)	(Axis-C)	0.49	1.44	1.56

and the present scheme becomes smaller as $\Delta r \to 0$.

6. CONCLUSIONS

Investigations were made on the energy conservation of second-order accurate finite difference schemes for cylindrical coordinate system. A combination of highly energy-conservative schemes for advection and centrifugal / Coriolis terms, and the treatment of the singularity at the cylindrical axis was proposed.

Similarly to the case of the Cartesian coordinate system, the energy-conservative scheme for advection terms can be formulated by using relevant interpolation schemes. However, unlike in the Cartesian coordinate system [9], the resulting form of the energy-conservative scheme differs from that of an intuitive scheme based on arithmetic average, even when the mesh is equally spaced.

The proposed schemes are tested numerically via simulations of inviscid flow. The highly energy-conservative nature and the high stability of the present schemes over other schemes are demonstrated.

The strict energy conservation discussed in the present paper may not be required for DNS of a fully developed turbulent flow, as indicated in Appendix A, where a very fine mesh is used and large physical dissipation takes place. However, the energy conservation will become important in many other situations such as LES using coarse mesh and DNS of statistically unstationary turbulent flow due, for example, to external control input.

APPENDIX A: DNS OF FULLY DEVELOPED TURBULENT PIPE FLOW

As an initial field in test computations, an instantaneous velocity field of a fully developed turbulent pipe flow was used. In this appendix, some results from DNS of turbulent pipe flow at $Re_\tau = u_\tau R/\nu = 180$ are presented to show the accuracy of the present computation.

For the discretization of governing equation, Eqs. (1) and (2), the methods proposed in the present study, i.e. (Div.-C), (Body-C) and (Axis-C) are used. The diffusion terms are spatially discretized using an ordinary second-order accurate finite difference and integrated in time using Crank-Nicolson scheme. The length of the computational domain is 10 R. The computational mesh is $96 \times 128 \times 256$ and stretched in r direction from $\Delta r^+ = 0.46$ (wall) to $\Delta r^+ = 2.99$ (center). The computational time step is $\Delta t^+ = 0.18$.

As representative quantities, profiles of the mean velocity and the RMS velocity fluctuations, the limiting behavior of Reynolds stresses and the budget of kinetic energy are shown in Fig. 9. The present results agree well with available DNS data. All the other quantities which are not shown here are also in good agreement, with slight differences in the vicinity of the wall, as in Fig. 9c, due to the difference of resolution.

Turbulence statistics, Reynolds stress budgets, two-point correlations and one-dimensional energy spectra computed by the present DNS are available in tabulated forms at the website (`http://www.thtlab.t.u-tokyo.ac.jp/`).

ACKNOWLEDGMENTS

This work was supported through the Project for Organized Research Combination System by the Ministry of Education, Culture, Sports and Technology of Japan (MEXT).

REFERENCES

[1] M. Lesieur, and O. Métais, New trends in large-eddy simulations of turbulence, *Ann. Rev. Fluid Mech.* **28,** 45 (1996).

[2] U. Piomelli, Large-eddy simulations: where we stand, in *Advances in DNS / LES* edited by Liu et al. (Greyden Press, Columbus, 1997), p. 93.

[3] N. Kasagi, Progress in direct numerical simulation of turbulent transport and its control, *Int. J. Heat Fluid Flow* **19,** 125 (1998).

[4] P. Moin, and K. Mahesh, Direct numerical simulation: a tool in turbulence research, *Ann. Rev. Fluid Mech.* **30,** 539 (1998).

[5] D. Gottlieb, and S. A. Orszag, *Numerical Analysis of Spectral Methods: Theory and Applications*, (Society for Industrial and Applied Mathematics, Philadelphia, 1977).

[6] F. H. Harlow, and J. E. Welch, Numerical calculation of time-dependent viscous incompressible flow of fluid with free surface, *Phys. Fluids* **8,** 2182 (1965).

[7] S. A. Piacsek, and G. P., Williams, Conservation properties of convection difference schemes, *J. Comput. Phys.* **6,** 392 (1970).

[8] Y. Morinishi, T. S. Lund, O. V. Vasilyev, and P. Moin, Fully conservative higher order finite difference schemes for incompressible flow, *J. Comput. Phys.* **143,** 90 (1998), doi:10.1006/jcph.1998.5962.

[9] T. Kajishima, Finite-difference method for convective terms using non-uniform grid, *Trans. JSME / B* **65 (633),** 103 (1999) (in Japanese).

[10] F. E. Ham, F. S. Lien, and A. B. Strong, A fully conservative second-order finite difference scheme for incompressible flow on nonuniform grids, *J. Comput. Phys.* **177,** 117 (2002), doi:10.1006/jcph.2002.7006.

[11] J. G. M. Eggels, F. Unger, M. H. Weiss, J. Westerweel, R. J. Adrian, R. Friedrich, and F. T. M. Nieuwstadt, Fully developed turbulent pipe flow: a comparison between direct numerical simulation and experiment, *J. Fluid Mech.* **268,** 175 (1994).

[12] K. Akselvoll, and P. Moin, Large eddy simulation of turbulent confined coannular jets and turbulent flow over a backward facing step, Stanford Univ. Report No. TF-63 (1995).

[13] R. Verzicco, and P. Orlandi, A finite-difference scheme for three-dimensional incompressible flows in cylindrical coordinates, *J. Comput Phys.* **123,** 402 (1996), doi:10.1006/jcph.1996.0033.

[14] P. Orlandi, and M. Fatica, Direct simulations of turbulent flow in a pipe rotating about its axis, *J. Fluid Mech.* **343,** 43 (1997).

[15] G. S. Constantinescu, and S. K. Lele, A new method for accurate treatment of flow equations in cylindrical coordinates using series expansions, in *CTR Annual Research Briefs 2000* edited by P. Moin et al. (Center for Turbulence Research, NASA Ames and Stanford University, 2000), p.199.

[16] K. Mohseni, and T. Colonius, Numerical treatment of polar coordinate singularities, *J. Comput. Phys.* **157,** 787 (2000), doi:10.1006/jcph.1999.6382.

[17] O. Vasilyev, High order finite difference schemes on non-uniform meshes with good conservation properties, *J. Comput. Phys.* **157,** 746 (2000), doi:10.1006/jcph.1999.6398.

[18] J. P. Boyd, *Chebyshev and Fourier Spectral Methods*, (Springer-Verlag, Berlin, 1989), p. 475.

[19] P. R. Spalart, R. D. Moser, and M. M. Rogers, Spectral methods for the Navier-Stokes equations with one infinite and two periodic directions, *J. Comput. Phys.* **96,** 297 (1991).

[20] M. M. Rai, and P. Moin, Direct numerical simulations of turbulent flow using finite difference schemes, *J. Comput. Phys.* **96,** 15 (1991).

[21] J. K. Dukowicz, and A. S. Dvinsky, Approximate factorization as a higher-order splitting for the implicit incompressible flow equations, *J. Comput. Phys.* **102,** 336 (1992).

[22] R. D. Moser, J. Kim, and N. N. Mansour, Direct numerical simulation of turbulent channel flow up to $Re_\tau = 590$. *Phys. Fluids* **11,** 943 (1999).

(a)

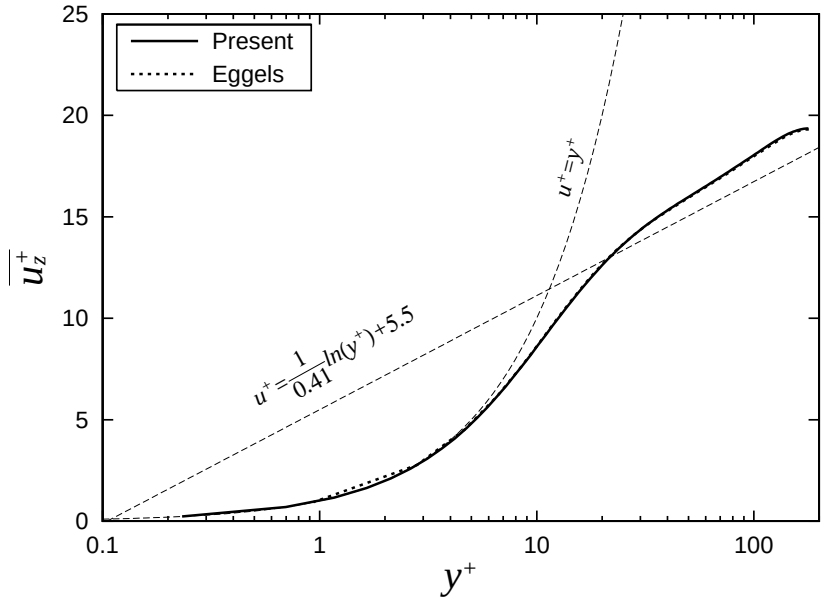

(b)

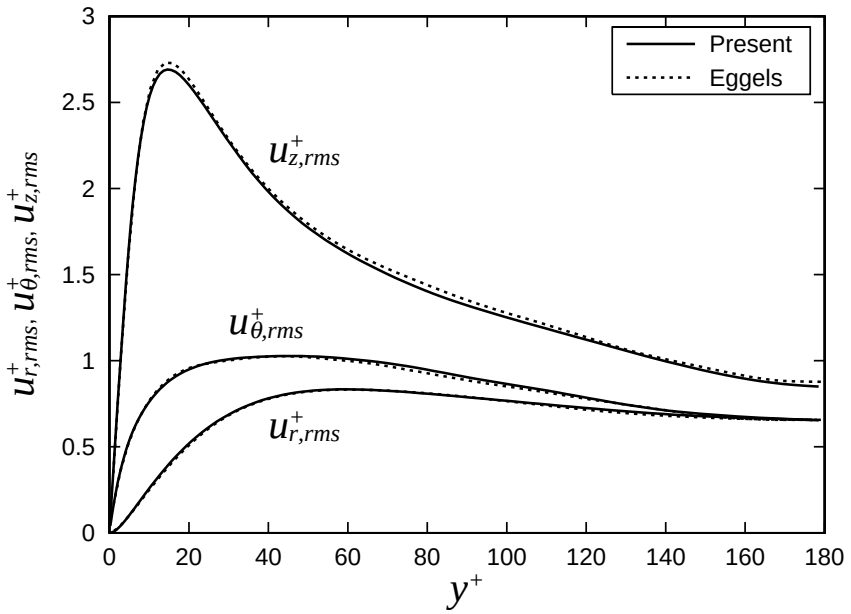

FIG. 9 — *Caption opposite.*

(c)

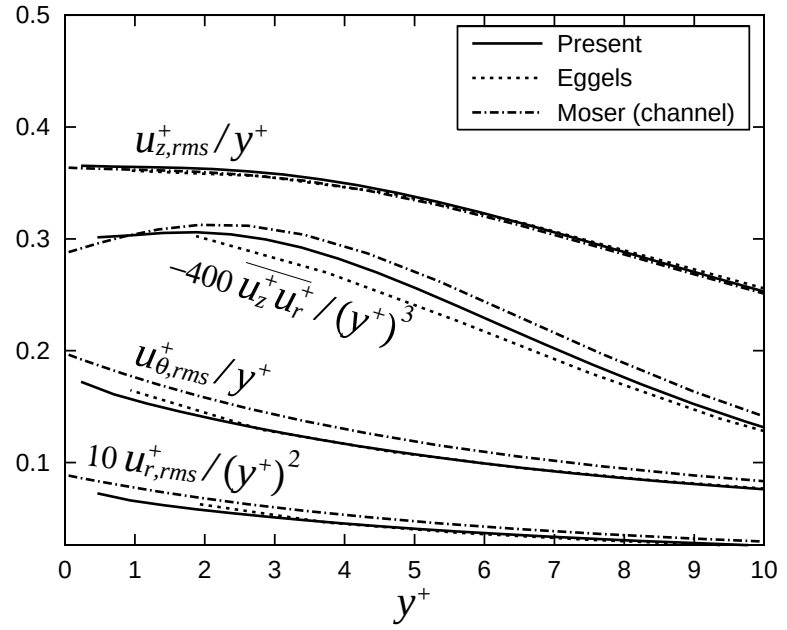

(d)

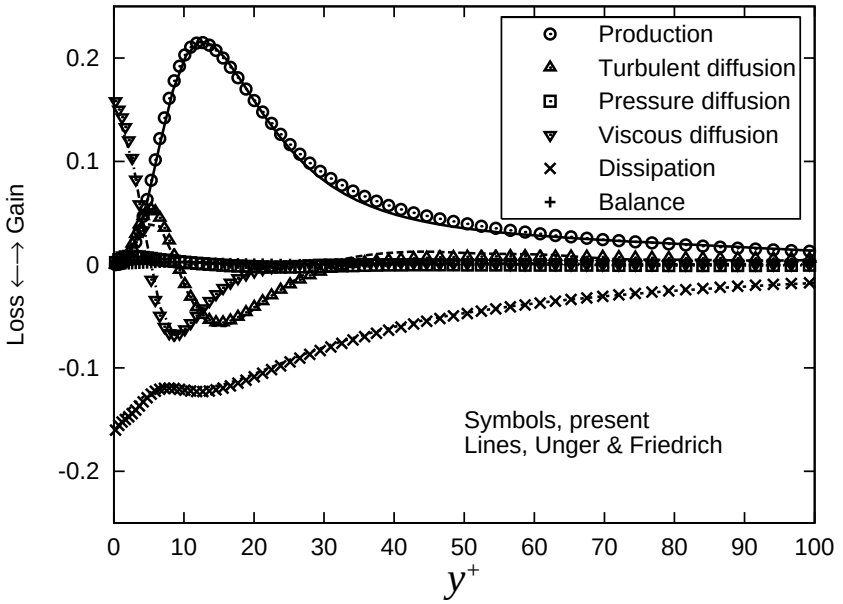

FIG. 9 Typical results from DNS of turbulent pipe flow at $Re_\tau = 180$. (a) Mean velocity profile; (b) RMS velocity fluctuations; (c) Limiting behavior of Reynolds stresses; (d) Turbulent kinetic energy budget. Present results are compared with DNS data by Eggels *et al.* (1994), Unger & Friedrich (in Eggels *et al.*, 1994) and DNS data of channel flow by Moser *et al.* (1999).